BEM-Computation of 3D Transient Scattering from Conducting Bodies

Erwin Schlemmer, Wolfgang M. Rucker and Kurt R. Richter

Institute for Fundamentals and Theory in Electrical Engineering
Graz University of Technology
Kopernikusgasse 24, A-8010 Graz, Austria

ABSTRACT

In this paper an overview of the mathematical foundations and boundary element formulation of the problem of transient electromagnetic scattering from conducting bodies is given. Starting from Maxwell's equations the basic integral equations are derived by applying Green's theorem for vector variables and the definition of the appropriate Green's function. In order to apply the BEM the discretization of the boundary into boundary elements is discussed. The problems arising by handling objects with edges or vertices are dealt with. Some results show the applicability of the method for three-dimensional transient scattering problems since the method exhibits robustness against late-time instabilities.

INTRODUCTION

A topic of some concern in target identification and electromagnetic compatibility is the interaction of electromagnetic pulses with conducting bodies. The increased use of wideband radar facilities has brought a demand for computer techniques which are capable of predicting some of the target's electromagnetic features.
An electromagnetic scattering problem in general is defined by a set of coupled partial differential equations and appropriate boundary and initial conditions. By defining a Green's function which satisfies the differential equation and the boundary conditions for a point source, the solution of the problem can be expressed as an integral over the known source function multiplied by Green's function. The differential equation can be transformed into an integral equation which has certain advantages in the solution of open boundary problems. The main benefits are that Green's function implicitly fulfills the radiation condition and so there is no need for an outer boundary or the use of an absorbing boundary condition. The discretization effort can be reduced from the modelization of the domain to the modelization of the surface under certain conditions (vanishing initial conditions, linear materials, ...). The resulting system of linear equations is therefore smaller as the system of a finite difference or finite element method. However, it is fully populated with respect to the retardation of the electromagnetic signals.
The integral methods used for scattering applications can be subdivided into frequency-domain methods and time-domain methods. The first of these involves the computation of the frequency-domain response of the structure which is subsequently Fourier transformed to yield the desired time-domain response.
The latter one, which will be employed in this paper, solves the problem in the time-domain by a time-stepping method with or without a matrix inversion algorithm, depending on the representation of the solution on the surface.
In the subsequent sections, we want to show how it is possible to expand the well known method of boundary element discretization (Brebbia, 1980) into the region of transient electromagnetic scattering problems. The new feature of the presented work is the application of semi-discontinuous boundary elements (Ingber, Ott, 1991) in the time-domain and the possibility of obtaining a stable solution via a matrix inversion technique (for stability see e.g. (Rynne, 1985)).

1. MATHEMATICAL FOUNDATIONS

1.1 The Magnetic Field Integral Equation (MFIE)

We shall restrict ourselves to the simplest case which is a conducting body supporting induced currents and charges only on its surface. For smooth conductors, the Magnetic Field Integral Equation (MFIE) (9) is employed since the geometrical factors often tend to make the contribution from the integral small compared to the contribution of the incident field. Fig. 1 shows the geometry which will be considered in the subsequent sections. Ju and J_v are u- and v-componentes of the surface current density supported by

a perfect conducting object. r and r' are the co-ordinates of the observation point and of the source point respectively. The boundary of the conducting region W is denoted by G and dG is a differential surface element.

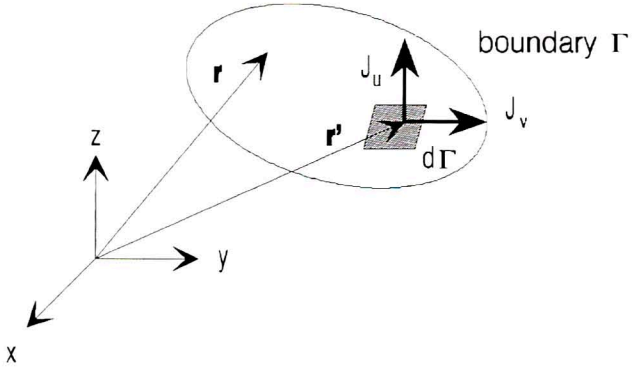

Fig. 1 - Geometry of a scatterer with differential surface element $d\Gamma$.

A scattering problem can be described by Maxwell's equations (1) and (2) where **H** is the magnetic field strength, **J** the (volume) current density, **E** the electric field strength, e the permittivity and m the permeability of the (linear and isotropic) medium.

$$\nabla \times \mathbf{H} = \mathbf{J} + \varepsilon \frac{\partial \mathbf{E}}{\partial t} \tag{1}$$

$$\nabla \times \mathbf{E} = -\mu \frac{\partial \mathbf{H}}{\partial t} \tag{2}$$

After some manipulation, we obtain the vector wave equation (3) for the magnetic field strength.

$$\nabla \times \nabla \times \mathbf{H} + \mu \varepsilon \frac{\partial^2 \mathbf{H}}{\partial t^2} = \nabla \times \mathbf{J} \tag{3}$$

It should be mentioned that several steps have been omitted for the sake of brevity. They can be found in full detail in (Felsen, 1976) and in (Mittra, 1973). The appropriate Green's function for this problem is defined via (4).

$$\nabla \times \nabla \times \mathbf{G} + \mu \varepsilon \frac{\partial^2 \mathbf{G}}{\partial t^2} = \mathbf{p}\, \delta(\mathbf{r} - \mathbf{r}')\, \delta(t - t') + \\ + \nabla (\nabla \cdot \mathbf{G}) \tag{4}$$

where

$$\mathbf{G} = \mathbf{p}\, G(\mathbf{r},\mathbf{r}' ; t,t') = \mathbf{p} \frac{\delta(t - t' R/c)}{4 \pi R} \tag{5}$$

and G is the solution of the three-dimensional scalar wave equation (Morse, Feshbach, 1953). **p** is an arbitrary vector, t is the time at the observation point and t' at the source point respectively. R is the distance between observation point and source point and c is the velocity of electromagnetic signal propagation defined by $c = (\varepsilon \mu)^{-1/2}$. All primed quantities refer to the source point, unprimed ones indicate the observation point. In the following analysis, primes will be used to indicate vector operations in source co-ordinates. Also, a prime will be used to indicate a normal defined at a source point.

Applying the vector equivalent of Green's theorem where all operations are performed in the source co-ordinates

$$\int_{t'=0}^{t^+} \iiint_{\Omega} \left\{ \mathbf{A} \cdot \nabla' \times \nabla' \times \mathbf{G} - \mathbf{G} \cdot \nabla' \times \nabla' \times \mathbf{A} \right\} d\Omega\, t' = \\ = \int_{t'=0}^{t^+} \iint_{\Gamma} \left\{ G \times \nabla' \times A - A \times \nabla' \times G \right\} \cdot n'\, d\Gamma\, dt' \tag{6}$$

we arrive after some manipulation which again can be found in (Mittra, 1973) at the magnetic field integral equation for perfect conducting bodies. In (6), t+ denotes t+e where e is a small time increment to avoid ending the integration at the peak of a delta-pulse (5).

$$T(\mathbf{r})\, \mathbf{n} \times \mathbf{H}(\mathbf{r}, t) = \mathbf{n} \times \mathbf{H}^{inc}(\mathbf{r}, t) \\ - \mathbf{n} \times \int_{t'=0}^{t^+} \iint_{\Gamma} (\mathbf{n}' \times \mathbf{H}(\mathbf{r}', t')) \times \nabla' \mathbf{G}(\mathbf{r}, \mathbf{r}' ; t, t')\, d\Gamma\, dt' \tag{7}$$

In (7) n denotes the unit vector normal to the boundary. H is the magnetic field vector, r the position vector and ∇ the del-operator. T(r) denotes the coefficient of the singularity which is 2 for points on a smooth surface and W/4p for points on an edge or a vertex with Ω the solid angle. The value of T(r) is dependent from what side of the boundary the excluded volume is seen and it is therefore different from that used in (Mittra, 1973). For a more detailed treatment of the step from the integral representation of the magnetic field strength to the integral equation for the surface current density, the reader is referred to the excellent discussion in (Mittra, 1973). With the surface current density

$$\mathbf{J} = \mathbf{n} \times \mathbf{H}$$

and time quadrature from t'=0 to t'=t+, equation (7) takes the form

$$T(\mathbf{r})\, \mathbf{J}(\mathbf{r}, t) = \mathbf{n} \times \mathbf{H}^{inc}(\mathbf{r}, t) + \\ - \mathbf{n} \times \frac{1}{4\pi} \iint_{\Gamma} \left\{ \left(\frac{1}{R^2} \frac{1}{Rc} \frac{\partial}{\partial t'} \right) \mathbf{J}(\mathbf{r}', t') \times \frac{\mathbf{R}}{\mathbf{R}} \right\} \Big|_{t' = t - R/c} d\Gamma \tag{9}$$

Equation (9) is the simplest vector integral equation due to the fact that only one unknown remains in the equation. It is obviously an integral equation of the second kind which is well suited for numerical approximation. The evaluation of the integrals does not pose severe problems because of the geometrical terms which make the kernel's singularity of order O(1/r) on a smooth boundary. On non-smooth boundaries, the normals are not uniquely defined at the geometrical singularity. So additional difficulties arise which have to be circumvented by moving the boundary nodes away from the geometric singularities (Ingber, Ott, 1991).

2. BOUNDARY ELEMENT FORMULATION

2.1 The BEM-Discretization of the MFIE

The numerical treatment of the boundary integral equation (9) can be performed by applying the boundary element method (BEM). This implies the discretization of the closed surface G of the considered region W into finite elements, the so-called boundary elements. There exists a widespread variety of possibilities to accomplish the modeling of a boundary G (Brebbia, 1980).

For the discretization of the boundary of a 3D problem quadrilateral elements of second order may be used. The transformation of such an element from the global to the intrinsic co-ordinate system is shown in fig. 2.

For the definition of a structure (the so-called macro structure) 9-noded elements are employed which can be subdivided automatically into 8-noded boundary elements in order to produce a finer mesh. The central node usually is neglected thus resulting in a smaller number of boundary nodes (Cheung, Yeo, 1979).

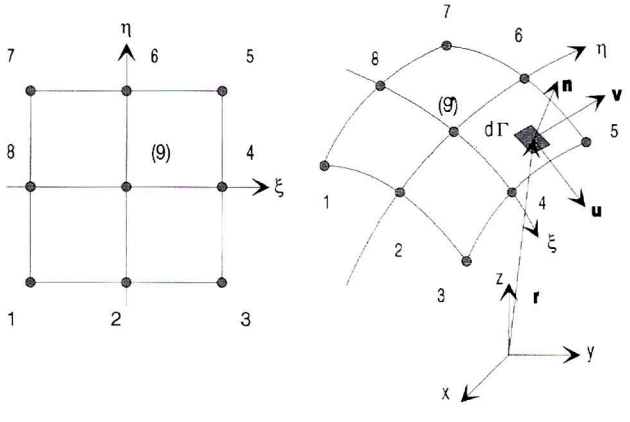

Fig. 2 - Principle of boundary-discretization using eight-noded elements.

The field quantities are also approximated by the same shape functions (isoparametric elements).

$$\mathbf{r}(\xi,\eta) = \sum_{k=1}^{8} N_k(\xi,\eta)\,\mathbf{r}_k \tag{10}$$

$$\mathbf{J}(\xi,\eta) = \sum_{k=1}^{8} N_k(\xi,\eta)\left\{\left[\alpha_k\,\mathbf{u}(\xi,\eta) + \beta_k\,\mathbf{v}(\xi,\eta)\right]J_{uk} + \left[\gamma_k\,\mathbf{u}(\xi,\eta) + \delta_k\,\mathbf{v}(\xi,\eta)\right]J_{vk}\right\} \tag{11}$$

The subscript k denotes the nodal value of a quantity at the boundary point k, ξ and η are the local co-ordinates, N_k is the shape function for node k. The terms α_k, β_k, γ_k, and δ_k are factors which take the different orientations of global node vectors and local source vectors into account. These factors are obtained via the following relations at the nodal points which are defined by their local co-ordinates (ξ_0, η_0).

$$\mathbf{u}_{k\,(glob)}\Big|_{\xi_0,\,\eta_0} = \alpha_k\,\mathbf{u}(\xi_0,\eta_0) + \beta_k\,\mathbf{v}(\xi_0,\eta_0) \tag{12}$$

$$\mathbf{v}_{k\,(glob)}\Big|_{\xi_0,\,\eta_0} = \gamma_k\,\mathbf{u}(\xi_0,\eta_0) + \delta_k\,\mathbf{v}(\xi_0,\eta_0) \tag{13}$$

Due to the isoparametric approximation of the boundary Γ, the element-based tangential vectors do not coincide in general with the global tangents which are computed using the mean value of the adjacent element-normals. The element-based tangentials are defined by (14) and (15), the local normal is the normalized cross product of the tangents.

$$\mathbf{u}(\xi,\eta) = \frac{\dfrac{\partial\,\mathbf{r}(\xi,\eta)}{\partial\,\xi}}{\left|\dfrac{\partial\,\mathbf{r}(\xi,\eta)}{\partial\,\xi}\right|} \tag{14}$$

$$\mathbf{v}(\xi,\eta) = \frac{\dfrac{\partial\,\mathbf{r}(\xi,\eta)}{\partial\,\eta}}{\left|\dfrac{\partial\,\mathbf{r}(\xi,\eta)}{\partial\,\eta}\right|} \tag{15}$$

The differential surface element can be calculated by (16), the surface integration in (17) is performed using Gauss' quadrature formula.

$$d\Gamma(\xi,\eta) = \left|\frac{\partial\,\mathbf{r}}{\partial\,\xi} \times \frac{\partial\,\mathbf{r}}{\partial\,\eta}\right| d\xi\,d\eta \tag{16}$$

The geometrical discretization transforms the boundary integral equation into a system of linear equations. Equation (9) can be written for the i-th field point as follows.

$$T_i(\mathbf{r}_i)\,\mathbf{J}_i(\mathbf{r}_i,t) = \mathbf{n}_i \times \mathbf{H}_i^{inc}(\mathbf{r}_i,t) - \mathbf{n}_i \times \sum_{j=1}^{N} \iint_{\Gamma_j} \left\{\mathbf{J}_j(\mathbf{r}_j,t') \times \mathbf{L}(R_{ij}\,t')\right\}\Big|_{t'=t-R/c} d\Gamma \tag{17}$$

$$\mathbf{L}(R_{ij}, t') = \frac{\mathbf{R}_{ij}}{R_{ij}} \left(\frac{1}{R_{ij}^2} + \frac{1}{R_{ij}\, c} \frac{\partial}{\partial\, t'} \right) \tag{18}$$

Considering all N nodes (i=1, ..., N) and all M time steps (l=1, ..., M) this procedure leads to a system of linear equations which can be written in matrix notation. The matrices $[\mathbf{A}_l]$ can be found from the time-discretized version of (17) where every time intervall t_l in the past (within the number L_{ret} (20) of time-steps which is given by the retardation of the electromagnetic signals) generates its matrix $[\mathbf{A}_l]$. The time axis has been subdivided into constant elements where a linear variation of the field quantities is assumed.

$$[\mathbf{A}_M]\,\{\mathbf{J}_M\} = \{\,\mathbf{n} \times \mathbf{H}_M^{inc}\,\} \; - \sum_{l\,=\,max\,(1\,,\,M\,-\,L_{ret})}^{M\,-\,1} [\mathbf{A}_M]\;\{\mathbf{J}_l\} \tag{19}$$

$$L_{ret} = int \left(\frac{max\,(R_{ij}/c)}{\Delta\, t} \right) + 1 \tag{20}$$

The right hand side of (19) contains only the incident field $\mathbf{H}_{inc}$ and already known values of the surface current density at past time instands. So (19) can be solved by building up the solution from previously calculated results employing a time stepping-procedure.

The use of eight-noded boundary elements results in a coupled system of equations that means a matrix inversion has to be carried out since all nodes within a distance $c\,\Delta\,t$ from the observation point are coupled with the latter. This inversion however makes the system stable against spurious oscillations which frequently occur in time-stepping procedures without matrix inversion.

It is well known that conventional time-stepping methods provide the solutions only for one aspect angle. But since we calculate the full matrix of coefficients and store it, we have no need to repeat the whole computation of the matrix' entries for different angles of incident. Thus, the solution is obtained by matrix multiplication of the (once inverted and stored) matrix of the uppermost time-step with the right hand side consisting of the vector of incident field values at the collocation points and of the already known current values at previous time-steps (multiplied with their element matrices representing the past). In this way, we get a behaviour which is comparable with frequency-domain methods.

2.2 Problems with Eight-Noded Boundary Elements

Although eight-noded boundary elements offer the possibility of an accurate description of geometry and field quantities, certain problems arise due to the non-smoothness of derivatives at the element contours.

The first one is that the globally defined normal and tangential vectors are not unique in a node-point because of the quadratic approximation of the body's shape. Fig. 3 sketches the problem.

On smooth boundaries the field quantities are defined using "global node-vectors" which are computed from the local normals of the adjacent elements (which have the node in common) using their mean value. In the surface integrals, the field quantities are represented by the local vectors weighted by factors which take the different orientation of global vectors and local vectors in the node point j into account.

Since the collocation points of the equation - the boundary nodes - are located directly on the contour of a boundary element, and the kernel of the integral is singular, the wrong choice of the vector n in (17) introduces an significant error in the computation fo the element matrix' entries.

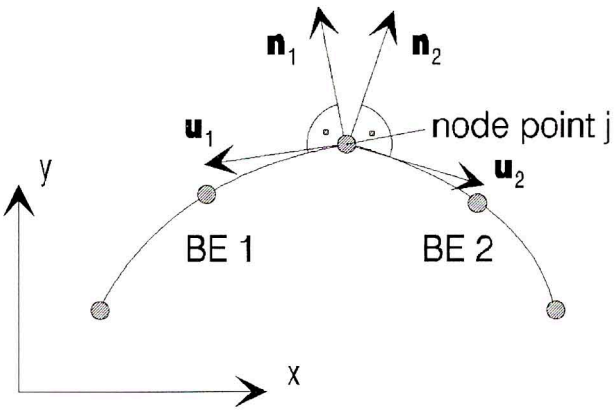

Fig. 3 - Surface vectors at an element-element interface (cross-section).

If the abovementioned vector is replaced by an element-based local normal, the singularity of the kernel can be reduced to the order of O(1/r) and the integration is performed without difficulty.

At sharp edges or vertices, some field quantities tend towards infinity although their energy contents has to remain finite e.g. (Felsen, Marcuvitz, 1973). Since the analytical behaviour of these fields is known in first approximation (Van Bladel, 1991) the nodes are moved away from the geometric singularity.

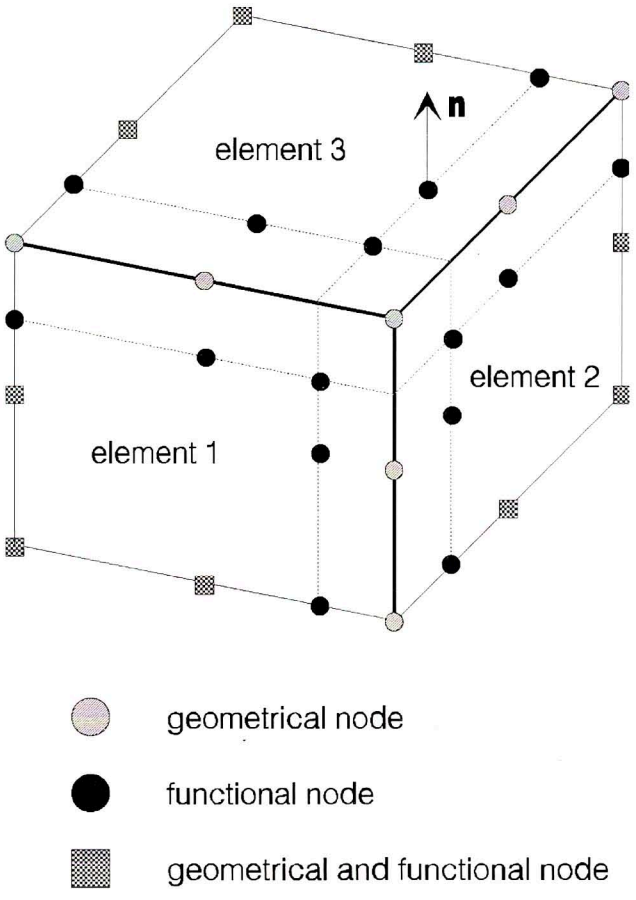

Fig. 4 - Corner of a cube with moved boundary element nodes.

This results in the use of semidiscontinuous elements (Ingber, Ott, 1991) which avoids also problems with non-unique surface vectors at edges and vertices. In the gap between the old and the new node position, the shape functions are weighted with Van Bladel's analytical solution. Fig. 4 shows a corner of a cube discretized with semidiscontinuous elements. The node positions of conventional isoparametric boundary elements were situated directly on the edges and on the vertex (now geometrical nodes used only for the description of the geometry). The values of the surface current density are described in the so-called functional nodes. On a smooth portion of the body geomtrical nodes and functional nodes coincide.

3. APPLICATIONS

3.1 The Perfect Conducting Sphere

This problem is one of the standard test problems for all scattering codes since its analytical solution is (at least in the frequency-domain since the beginning of our century) known, although it does not say anything about the behaviour of the method in the case of sharp edges or corners. We wish to state that impulse scattering from a sphere has been published as a test case from nearly every author dealing with this topic since the work of Bennett in the late 1960s, e.g. (Uslenghi, 1978). Therefore, this example is given here to show how good our results coincide with analytical ones. Our chief aim was to show how to obtain a numerical stable solution and how to deal with sharp edges and vertices in the time-domain using higher order boundary elements which (to our knowledge) is a relatively new topic.

Due to the smoothness of the boundary, all kernels are of the order O(1/r) and so, numerical integration does not pose problems if the normals are carefully chosen.

As obstacle serves a perfect conducting sphere of diameter d=2m, the pulsewith of the incident Gaussian pulse (21) is of the order of twice the sphere's diameter.

$$\mathbf{H}^{inc} = \mathbf{H}_0^{inc}\ e^{-\left[\frac{p\,(r - r_0) - c\,(t - t_0)}{a}\right]^2} \tag{21}$$

p is a unit vector normal to the wavefront and a is a decay parameter. At a distance of 2a from the pulse's peak, the magnitude has fallen to about 2% of $\mathbf{H}_0^{inc}$. The value of a was chosen to be 1m.

Fig. 5 shows the surface current density at two equatorial points, the front-point 1 and the side-point 2. The results were compared with the analytical solution in point 2 (thick points in fig. 5 over the dashed line) obtained by Bennett via the Mie series solution in the frequency domain and subsequent Fourier transform which was published by (Rao, Wilton, 1991). The peak value of the incident wave used of Rao and Wilton has been scaled to 1 A/m. The agreement between our solution and the analytical one is very good. Our solution shows no instabilities for late times, even for coarse discretization. At this point we want to emphasise the difference between our approach and that of Rao and Wilton. They use the EFIE which has the advantage to be valid even at plane structures such as a flat plate, however, they have to deal with an integral equation of the first kind where the computation of the self patches is essential for the solution and can be complicated. So they have to calculate the surface divergence of the electric surface current density via the shape functions which introduces charge doublets on two adjacent elements. These charge doublets may be a reason for their need of a high discretization and the instabilities in time which occur at relatively early times. In fig. 5, the magnitude of the tangential component of the incident magnetic field at the point 1 is shown as J_1^i (22).

$$\mathbf{J}_1^i = \left| \mathbf{n} \times \mathbf{H}^{inc}(\mathbf{r}_1, t) \right| \tag{22}$$

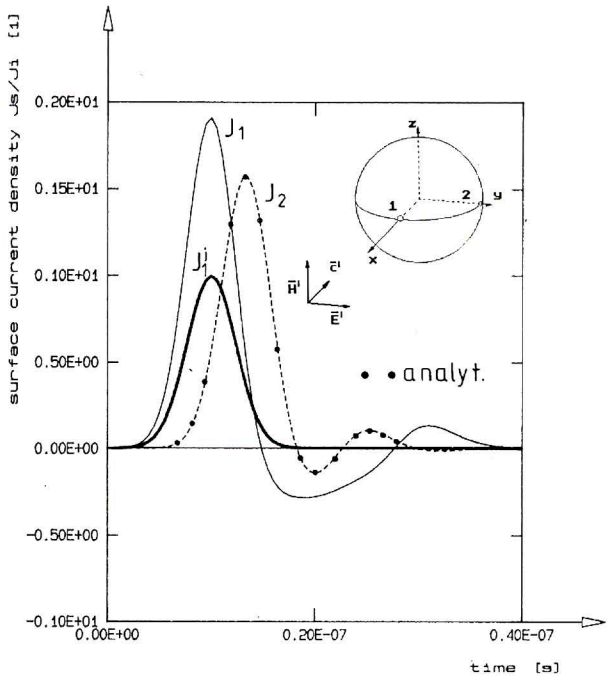

Fig.5 - Time variation of the electric surface current density at front-point 1 (solid line) and at side-point 2 (dashed line). Thick dots on the dashed line: analytical solution via Mie series and Fourier transform obtained by Bennett and published recently by (Rao, Wilton, 1991). Thick line: magnitude of the tangential component of the incident magnetic field strength. Inset: scatterer geometry with incident field vectors.

3.2 The Perfect Conducting Cube

A more interesting problem is the scattering of a pulse from a body with edges and corners, e.g. a metallic cube. As we move the boundary nodes away from the geometrical singularities, problems with not uniquely defined normals are avoided. As an incident pulse serves again (21) with a=2m. The results are compared with a BEM package based on the use of constant elements also developed at our institute (which is, of course, a well known approach). That means the field quantities are assumed to be constant over a whole element. The observation points are therefore located in the centre of the element and so no problems with nonunique vectors occur. The main disadvantage of the constant elements is that a great number of them is necessary in order to obtain an accurate solution.

Fig. 6 shows the electric surface current density at two points of the surface, front point 1 and side point 2 (solid line and dashed line). At the same points, the surface current density was computed using constant elements (thin dotted lines in the vicinity of the solid and the dashed line resp.). The two solutions show good agreement, although the package with constant elements uses only 25 patches per cube-face which is a rather coarse discretization. To avoid instabilities, the constant package also employs a matrix inversion technique coupling a certain number of surface patches per time-step.

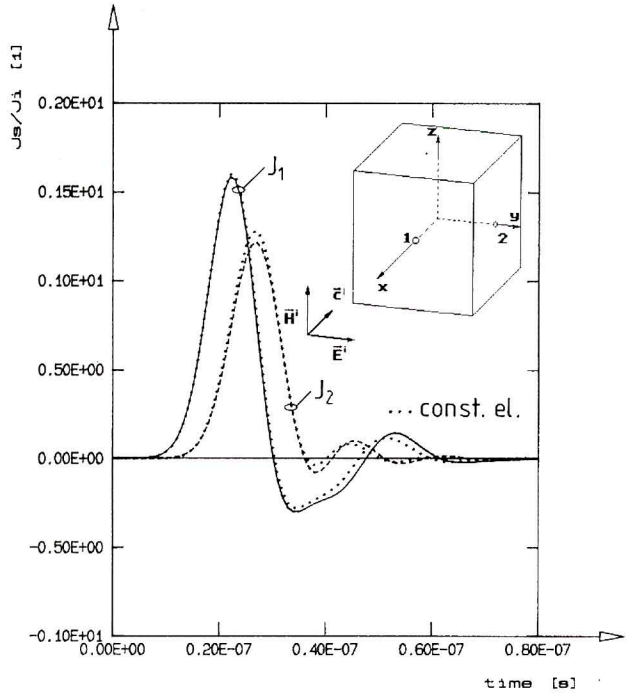

Fig. 6 - Time variation of the electric surface current density at front-point 1 (solidline) and at side-point 2 (dashed line). Dotted lines close to the solid and the dashed line: solutions at the same points obtained via a BEM package using constant elements. Inset: scatterer geometry with incident field vectors.

3.3 Computation of Scattered Fields

Although the comparison of surface current densities is the most interesting topic from a modeller's viewpoint since it exhibits the value of a solution in the most impressive way, remote sensing applications require the computation of scattered far-fields. This re-radiated fields can be calculated using the integral representation for the total magnetic field strength H (23) with the coefficient T(r) of the singularity from eq. (7) set equal to 1 (Mittra, 1973; Felsen, 1976). The scattered magnetic field H^s is obviously the surface integral over the induced surface current density J multiplied by Green's function.

$$\mathbf{H}(\mathbf{r},t) = \mathbf{H}^{inc}(\mathbf{r},t) + \mathbf{H}^{s}(\mathbf{r},t) = \mathbf{H}^{inc}(\mathbf{r},t) - \frac{1}{4\pi} \iint_{\Gamma} \left\{ \left(\frac{1}{R^2} + \frac{1}{Rc}\frac{\partial}{\partial t'} \right) J(r',t') \times \frac{R}{R} \right\} \Big|_{t'=t-R/c} d\Gamma \qquad (23)$$

The computation of the scattered electric fields requires the integral representation of the EFIE (Mittra, 1973; Felsen, 1976) employing the surface divergence of the surface current density which is not easy to obtain for a general co-ordinate system. Therefore the normal component of the electric field at the scatterer's surface should be computed via a weak formulation of the surface divergence of J incorporated into the integral equations. This, however, increases the number of unknowns.

In addition to the sphere and the cube, a cylinder and a pair of spheres have been calculated. The cylinder has a diameter of d=2m and the same height h. Its axis has the same orientation as the incident magnetic field. The spheres are placed one behind the other. The spacing between their mid-points is s=3m and the spheres' diameter is again d=2m. The decay parameter a was chosen to be 2m.

In the time-domain, scattering centres can be located directly from the far-field response. For two spheres, one observes roughly double the number of backswings as for the single sphere. From the run-time differences the distance between scattering centres can be estimated.

As to be expected, the cylinders's scattered field magnitude of the specular return is between those of sphere and cube, according to the sizes of the reflecting front portions. The cube's creeping wave return has the longest delay due to its larger circumference.

Figs. 7 and 8 show the backscattered magnetic field strength in the far-field zone for the abovementioned obstacles. The backscattered field has been scaled in the usual way with respect to R/a where R is the distance between the observation point and the origin of the scatterer's co-ordinate system, and a is the decay parameter of the incident Gaussian field. On the abscissa, the far-field time in light meters is shown. The far-field time is defined as ct-R and a far-field time of 0 corresponds to the time at which a signal sent from the co-ordinate origin (R=0) at (t=0) arrives at the far-field observation point.

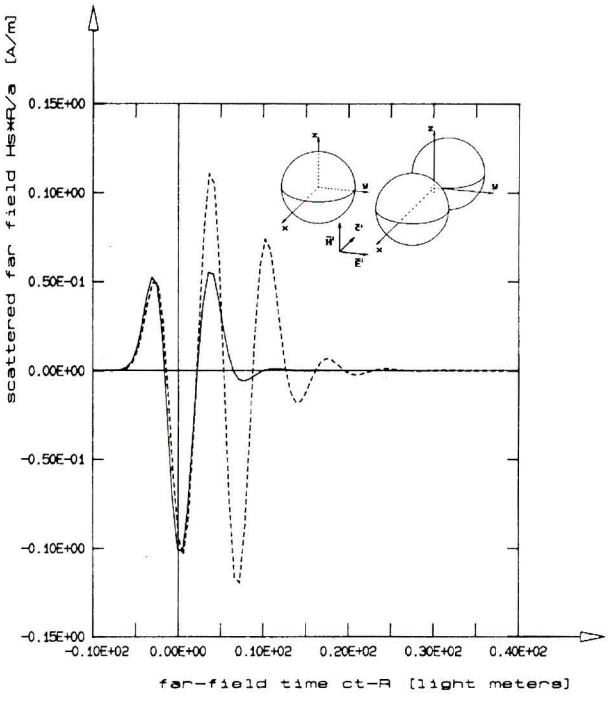

Fig. 7 - Magnetic far-fields in the backscattering direction. Solid line: sphere with diameter d=2m. Dashed line: two spheres with diameter d=2m and a spacing of s=3m between their mid-points. Inset: geometry of the scatterers.

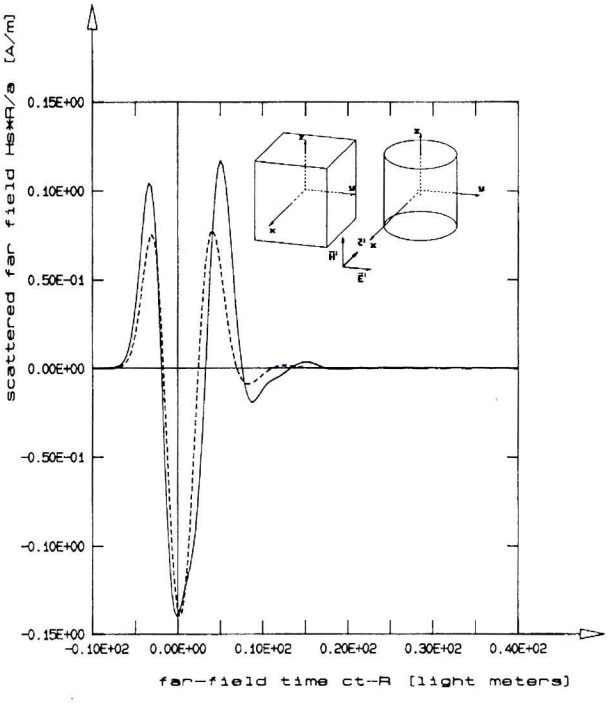

Fig. 8 - Magnetic far-fields in the backscattering direction. Solid line: cube with sidelength d=2m. Dashed line: Right circular cylinder with diameter and height d=h=2m.

CONCLUSION

The magnetic field integral equation was solved in the time domain for the case of arbitrary shaped conducting objects. It was shown how the boundary of the scatterer can be discretized and how the electric surface current density can be approximated using eight-noded quadrilateral boundary elements of second order. The problems arising with sharp edges and corners have been discussed. The presented examples show the applicability of the method.

ACKNOWLEDGEMENTS

This work was supported in part by the Austrian "Fonds zur Fvrderung der wissenschaftlichen Forschung" under Grant no. P8561-TEC.
The comments and additional references of the reviewers are gratefully acknowledged. However, we were not able to get all the articles in time.

REFERENCES

Brebbia, C.A., Walker, S., 1980, Boundary Element Techniques in Engineering (London: Newnes-Butterwords).

Cheung, Y.K., Yeo, M.F., 1979, A Practical Introduction to Finite Element Analysis (London: Pitman).

Felsen, L.B., Marcuvitz, N., 1973, Radiation and Scattering of Waves (Englewood Cliffs: Prentice-Hall).

Felsen, L.B. (Ed.), 1976, Transient Electromagnetic Fields (Berlin, Heidelberg, New York: Springer-Verlag).

Ingber., M.S., Ott, R.H., 1991, An Application of the Boundary Element Method to the Magnetic Field Integral Equation, IEEE Transactions on Antennas and Propagation, vol. 39, no. 5, pp. 606-611, May 1991.

Mittra, R. (Ed.), 1973, Computer Techniques for Electromagnetics (Oxford: Pergamon Press).

Morse, P.M., Feshbach. H., 1953, Methods of Theoretical Physics (New York: McGraw-Hill).

Rao, S.M., Wilton, D.R., 1991, Transient Scattering by Conducting Surfaces of Arbitrary Shape, IEEE Transactions on Antennas and Propagation, vol. 39, no.1, pp. 56-61, January 1991.

Rynne, B.P., 1985, Stability and Convergence of Time Marching Methods in Scattering Problems, IMA Journal of Applied Mathematics, vol. 35, pp 297-310, 1985.

Uslenghi, P.L. (Ed.), 1978, Electromagnetic Scattering (New York: Academic Press).

Van Bladel, J., 1991, Singular Electromagnetic Fields and Sources (Oxford: Claredon Press).